

Polynya Signature Simulation Method polynya area in comparison to AMSR-E 89 GHz sea-ice concentrations in the Ross Sea and off the Adélie Coast, Antarctica, for 2002–05: first results

Stefan KERN,¹ Gunnar SPREEN,¹ Lars KALESCHKE,²
Sara DE LA ROSA,¹ Georg HEYGSTER²

¹Center for Marine and Atmospheric Science, Institute of Oceanography, University of Hamburg,
Bundesstrasse 53, D-20146 Hamburg, Germany
E-mail: stefan.kern@zmaw.de

²Institute of Environmental Physics, University of Bremen, Otto-Hahn-Allee 1, D-28334 Bremen, Germany

ABSTRACT. The Polynya Signature Simulation Method (PSSM) is applied to Special Sensor Microwave/Imager observations from different Defense Meteorological Satellite Program spacecraft for 2002–05 to analyze the polynya area in the Ross Sea (Ross Ice Shelf polynya (RISP) and Terra Nova Bay polynya (TNBP)) and off the Adélie Coast (Mertz Glacier polynya (MGP)), Antarctica, on a sub-daily scale. The RISP and the MGP exhibit similar average total polynya areas. Major area changes ($>10\,000\text{ km}^2$; TNBP: $>2000\text{ km}^2$) occur over a range of 2–3 to 20 days in all regions. Sub-daily area changes are largest for the MGP (5800 km^2) and smallest for the TNBP (800 km^2), underlining the persistence of the forcing of the latter. ARTIST sea-ice (ASI) algorithm concentration maps obtained using 89 GHz Advanced Microwave Scanning Radiometer (AMSR-E) data are compared to PSSM maps, yielding convincing agreement in the average, similarly detailed winter polynya distribution. Average ASI algorithm ice concentrations take values of 25–40% and 65–80% for the PSSM open-water and thin-ice class, respectively. The discrepancy with expected values (0% and 100%) can be explained by the different spatial resolution and frequency used by the methods. A new land mask and a mask to flag icebergs are introduced. Comparison of PSSM maps with thermal ice thickness based on AVHRR infrared temperature and ECMWF ERA-40 data suggests an upper thickness limit for the PSSM thin-ice class of 20–25 cm.

1. INTRODUCTION

Investigating the ocean–atmosphere heat exchange and water-mass transformation in regions covered by sea ice requires knowledge of its distribution and thickness. Of particular interest in this context are polynyas, which are sites of intensive ocean–atmosphere heat exchange during winter, and can therefore be regarded as ice-production factories (Lemke, 2001). They act as a source for dense water feeding the Antarctic Bottom Water (e.g. Marsland and others, 2004). The influence of wintertime ice production and dense-water formation in coastal polynyas in the Southern Ocean on the global water mass distribution has been demonstrated (e.g. Stössel and Markus, 2004).

Our study focuses on polynyas in the Ross Sea and off the Adélie Coast, Antarctica: the Ross Ice Shelf polynya (RISP), the Terra Nova Bay polynya (TNBP) and the Mertz Glacier polynya (MGP), all being studied to some extent by modeling and remote sensing (Massom and others, 1998; Van Woert, 1999; Marsland and others, 2004; Ohshima and others, 2005). Satellite microwave radiometry has proven to be an excellent tool to study the location and development of polynyas in the Southern Ocean (Gordon and Comiso, 1988; Markus and others, 1998). The first study estimates the polynya area using a concentration threshold applied to sea-ice concentrations close to the coast. The second study is based on the Polynya Signature Simulation Method (PSSM) by Markus and Burns (1995). The advantage of the PSSM is that it uses an iterative surface-type classification instead of calculating the sea-ice concentration with one of the

standard algorithms (e.g. NASA-Team algorithm). Thereby errors in the polynya area due to false ice-concentration values are avoided. One alternative would be to use the Thin-Ice algorithm of Cavalieri (1994). This algorithm would, however, miss small-scale polynyas due to a much coarser spatial resolution as compared to the PSSM. Recently, a simple threshold-based approach was developed by Ohshima and others (2005). We present a multi-sensor study of the wintertime dynamics of the RISP, TNBP and MGP. For all three polynyas a time series of the polynya area, and the associated open-water and thin-ice fractions, is obtained by applying the PSSM to single overpass Special Sensor Microwave/Imager (SSM/I) data obtained from different spacecraft of the Defense Meteorological Satellite Program (DMSP) for the winters (April–September) of 2002–05. This time series is compared to sea-ice concentration estimates based on Advanced Microwave Scanning Radiometer (AMSR-E) data. A comparison to Advanced Very High Resolution Radiometer (AVHRR, from NOAA-16)-derived thickness estimates is carried out. The goal of the paper is to investigate:

- Which effects must be taken into account when using the PSSM to obtain polynya area time series?
- At what ice thickness do the PSSM thin-ice areas terminate?
- What additional information can we obtain from high-resolution AMSR-E 89 GHz ice-concentration estimates?

2. DATA AND TECHNIQUES

2.1. Polynya Signature Simulation Method (PSSM)

The PSSM was developed by Markus and Burns (1995) and refined by Hunewinkel and others (1998). The method is based on polarization ratios (vertically minus horizontally polarized brightness temperature divided by their sum) observed by the SSM/I at 37.0 and 85.5 GHz. It combines the finer spatial resolution at 85.5 GHz (field of view 13 km × 15 km, sampling distance 12.5 km) with the lower weather influence at 37.0 GHz (field of view 29 km × 37 km, sampling distance 25 km) in an iterative approach, in which the spatial distribution of three surface classes (open water, thin ice and thick ice) is obtained (see Fig. 1 for two examples). This distribution gives the total polynya extent (open water plus thin ice) and the areas occupied by open water and thin ice. The polynya extent can be estimated with a mean accuracy of 80 km². Changes in extent of 50 km² are observable (Markus and Burns, 1995; Hunewinkel and others, 1998), provided that the SSM/I data are interpolated onto a grid with 12.5 km × 12.5 km (37.0 GHz) and 5 km × 5 km (85.5 GHz) gridcell size. The PSSM has been applied in a number of studies (e.g. Markus and others, 1998; Martin and others, 2004b; Kern and others, 2005).

2.2. AMSR-E sea-ice concentrations

Brightness temperature observations at 89 GHz obtained from the AMSR-E on board NASA's Aqua satellite are used to calculate sea-ice concentrations on a grid with 6.25 km resolution. AMSR-E's 89 GHz channels offer today's highest spatial resolution passive microwave dataset with a complete daily coverage of the polar regions. A disadvantage is the enhanced atmospheric influence at this frequency in comparison to the lower-frequency channels at 19 and 37 GHz which are traditionally used for sea-ice concentration retrieval. Thus special attention must be paid to the elimination of spurious ice in the open ocean caused by cloud liquid water and water vapor in the atmosphere when using 89 GHz channels. We use the ARTIST (Arctic Radiation and Turbulence Interaction Study) Sea Ice (ASI) algorithm (Kaleschke and others, 2001; Spreen and others, in press), which is based on the ideas of Svendsen and others (1987), to calculate mean daily sea-ice concentrations. The algorithm makes use of the fact that the difference between vertically and horizontally polarized brightness temperatures near 90 GHz is typically large for open water and small for all ice types independent of season. Two tie points for the polarization difference of 100% and 0% ice cover including a standard high-latitude atmosphere are used to define a third-order polynomial, which models the development of sea-ice concentrations between 0% and 100%. Combinations of AMSR-E brightness temperatures obtained at frequencies of 19, 24 and 37 GHz are used to filter out spurious ice in the open ocean (Kaleschke and others, 2001; Spreen and others, in press). Examples are shown in Figure 1.

2.3. Sea-ice thickness

Different methods exist to estimate the thickness of thin ice from satellite infrared (IR) data (e.g. from the US National Oceanic and Atmospheric Administration (NOAA) Advanced Very High Resolution Radiometer (AVHRR)) or, more recently, also from satellite microwave radiometry (Martin and others, 2004a). We use the method of Drucker

and others (2003) (described in more detail in Yu and Lindsay, 2003), which is based on AVHRR IR data and the assumption that the thickness-dependent heat transfer through thin ice can be related linearly to its thickness. This way the thickness (thermal ice thickness) can be derived from the total heat flux at the surface, the under-ice water temperature and the surface temperature. Required quantities are the surface temperature and the air temperature, wind speed and humidity at 2 m height. We restrict our investigation to winter (April–September) and can neglect shortwave radiation. The total heat flux is then given by the sum of the up- and downwelling longwave radiation, and the turbulent sensible and latent heat fluxes. Surface temperatures are calculated from clear-sky IR surface temperature observations of AVHRR channels 4 and 5 following Key and others (1997) using the CASPR software (Key, 2002). Air temperature and wind speed are taken from the European Centre for Medium-Range Weather Forecasts (ECMWF) ERA-40 dataset using the 6 hourly analysis (Kållberg and others, 2004). The relative humidity is set constant to 90% following Yu and Lindsay (2003). These quantities and the derived surface temperature are used to calculate the mentioned heat fluxes following the equations given in Yu and Lindsay (2003). The under-ice water temperature and the conductivity of ice are set constant to -1.8°C and 2.03 W m K^{-1} , respectively. This approach neglects the influence of a potential snow cover and the sea-ice salinity. An error analysis by Drucker and others (2003) revealed a relative accuracy of the thermal ice thickness of about 20% for values below about 50 cm. Using 2002 as a test year, we calculated the ice thickness for all NOAA-16 AVHRR IR surface temperature observations with a considerable clear-sky area over the RISP and TNBP (approximately 50 cases). Figure 1 gives two examples of the distribution of the thermal ice thickness in the Ross Sea. Ice-thickness values are colour-coded as given by the legend. Negative ice-thickness values, values above 50 cm, clouds and bad values are flagged with different grey values (see Fig. 1 caption).

The two examples given in Figure 1 show reasonable clear-sky areas and an ice-thickness distribution, which agrees with the associated polynya distribution obtained with the PSSM and identified in the ASI algorithm ice-concentration maps. On 27 June, a polynya has just opened north of iceberg C19. The thin-ice map derived from AVHRR data, as well as the PSSM map and the ASI ice concentration reveal a small polynya. Note that ASI algorithm ice concentrations take values around 70% over the icebergs (see Fig. 1, upper left panel). On 3 July, a large polynya has developed, stretching over almost 100 km from the iceberg C19 northward. The thermal ice-thickness map shows a large area of ice with 15 cm thickness or less. The PSSM polynya area agrees quite well with this area, as does the area with reduced (down to 25%) ASI algorithm ice concentration. However, not all thin-ice areas in the thickness maps show up in the PSSM map, and not all such areas in the PSSM map show up in the thickness maps. There are three reasons for this. Firstly, PSSM maps are independent of a cloud cover, in particular of the frequently occurring fog; therefore the TNBP can be identified in the PSSM map but not in the thickness map on 27 June. Secondly, PSSM maps cannot show as many details as the thermal ice-thickness maps, due to the finer spatial resolution of the latter. Finally, the coarse spatial resolution of the ERA-40 data limits the accuracy of the

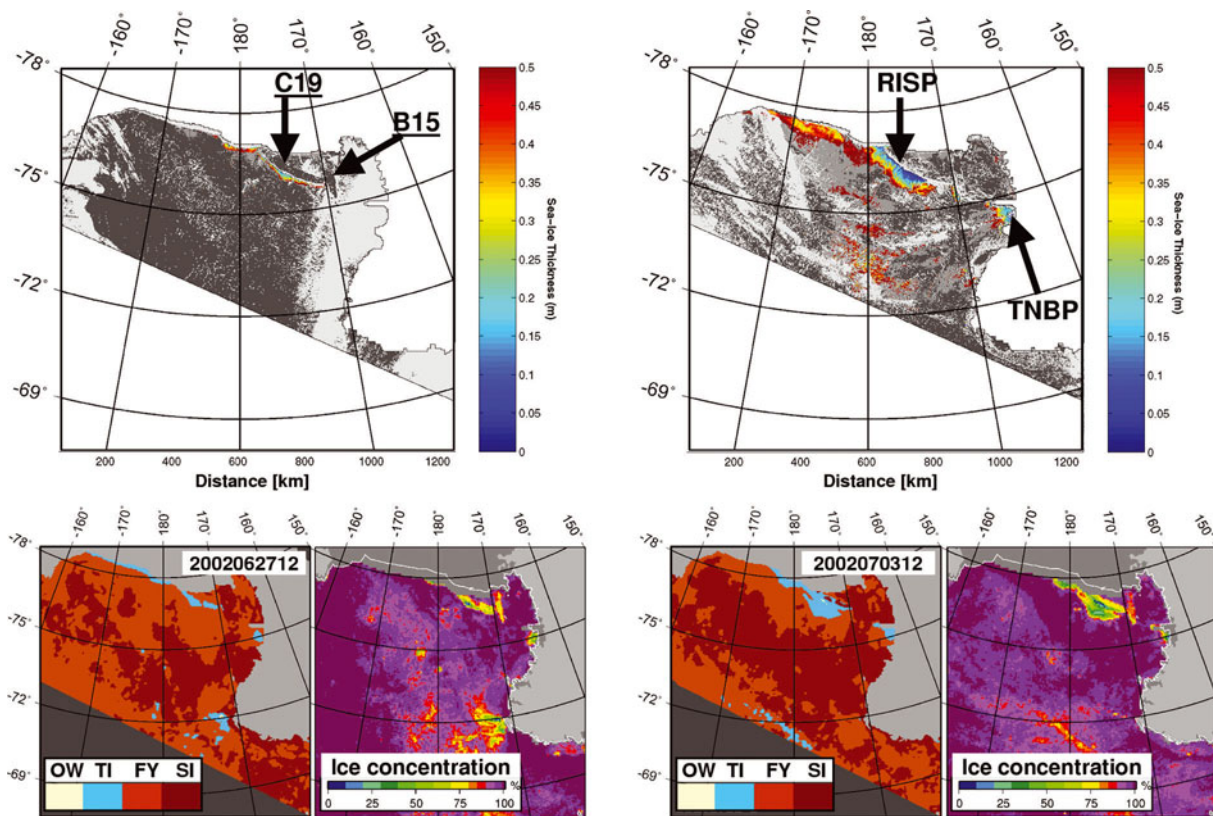


Fig. 1. Top row: Sea-ice thickness calculated with the method of Drucker and others (2003) (see text) from AVHRR images for 27 June, 11:44 UTC (left) and 3 July, 12:19 UTC (right), 2002. Size of the area is 1250 km \times 1250 km; grid spacing is 1 km. Land and missing data are marked white, clouds (obtained using the CASPR toolbox (Key, 2002)) are marked light grey, and negative ice-thickness values and thickness values above 0.5 m are given in dark and medium grey. The locations of the tabular icebergs C19 and B15 are indicated in the left panel. Bottom row: PSSM maps of the polynya distribution and the ASI algorithm sea-ice concentration for 27 June (left) and 3 July (right). The size of 1250 km \times 1250 km, and PSSM map (ice-concentration) grid spacing of 5 km (6.25 km) is valid for all subsequent maps of the Ross Sea. PSSM maps are within 1 hour time difference to the AVHRR image (2002062712 = yyyyymmddhh with yyyy = year, mm = month, dd = day and hh = hour); ice-concentration maps are of the same day. PSSM maps show open water (OW), thin ice (TI), thick ice (FY = 'normal' first-year ice, and SI = stable ice; see section 4), and land and missing data (medium and dark grey).

thickness retrieval. Particularly over inhomogeneous sea-ice areas such as polynyas and leads, ERA-40 air temperatures might be too low. This would cause an overestimation of the sensible heat flux and the total heat flux, and consequently an underestimation of the ice thickness. Certainly, there are other error sources, such as an insufficient cloud mask in the AVHRR data based surface temperature map and a general discrepancy between the real and the modelled near-surface meteorological conditions.

3. COMPARISONS

This section compares the PSSM and the ASI algorithm for the winters of 2002–05. Figure 2 shows a sample set of PSSM maps of the polynya distribution in the Ross Sea for 20–22 June 2002, together with daily average ASI algorithm sea-ice concentrations obtained from AMSR-E 89 GHz data. For each day, two PSSM maps are based on DMSP-f15 (11/12 and 18 UTC) and two on DMSP-f13 (9 and 15/16 UTC) SSM/I data. This way the study area receives four complete overpasses. The time given on each PSSM panel (for date format see Fig. 1 caption) is the SSM/I overpass time rounded to the nearest full hour. The period starts with a well-developed polynya in the lee of iceberg C19 and off the Ross Ice Shelf on 20 June 2002. The ASI algorithm captures essentially all polynya or thin-ice areas detected by the

PSSM as areas of reduced ice concentration. Note that the used AMSR-E land mask (adopted from the 12.5 km grid resolution AMSR-E data distributed by the US National Snow and Ice Data Centre (NSIDC), Boulder, CO) shows a too far northward extent of the Ross Ice Shelf. Parts of the RISPs are therefore missed by the ice-concentration map (green ellipses in middle row of Fig. 2). The same is true for the TNBP. The centre of the polynya shifts to the east on 21 June. During 22/23 June the polynya closes and it is closed on 24 June (not shown). Note the disappearance of the polynya at Cape Adare between 21 and 22 June (blue box in middle and bottom row of Fig. 2), which is identified by both methods. The PSSM maps encounter problems in the presence of icebergs (see Fig. 1), because the 85 GHz polarization ratio observed here is similar to that of thin ice; these problems can be mitigated using a special filter (see section 4). Evidently, the same is true for the ASI algorithm: ice concentrations are 70–95% over such icebergs (cf. Fig. 1).

Figure 3 shows a set of PSSM maps of the MGP region (SSM/I data from DMSP-f13 (hour (hh): 9 or 10, and 18 or 19) and -f15 (hh: 13 or 14, and 22)) for 26 and 27 June 2002, together with the daily average ASI algorithm sea-ice concentration of the same days. This example illustrates how fast polynya area, location and orientation can change in the MGP region: On 26 June the polynya located directly

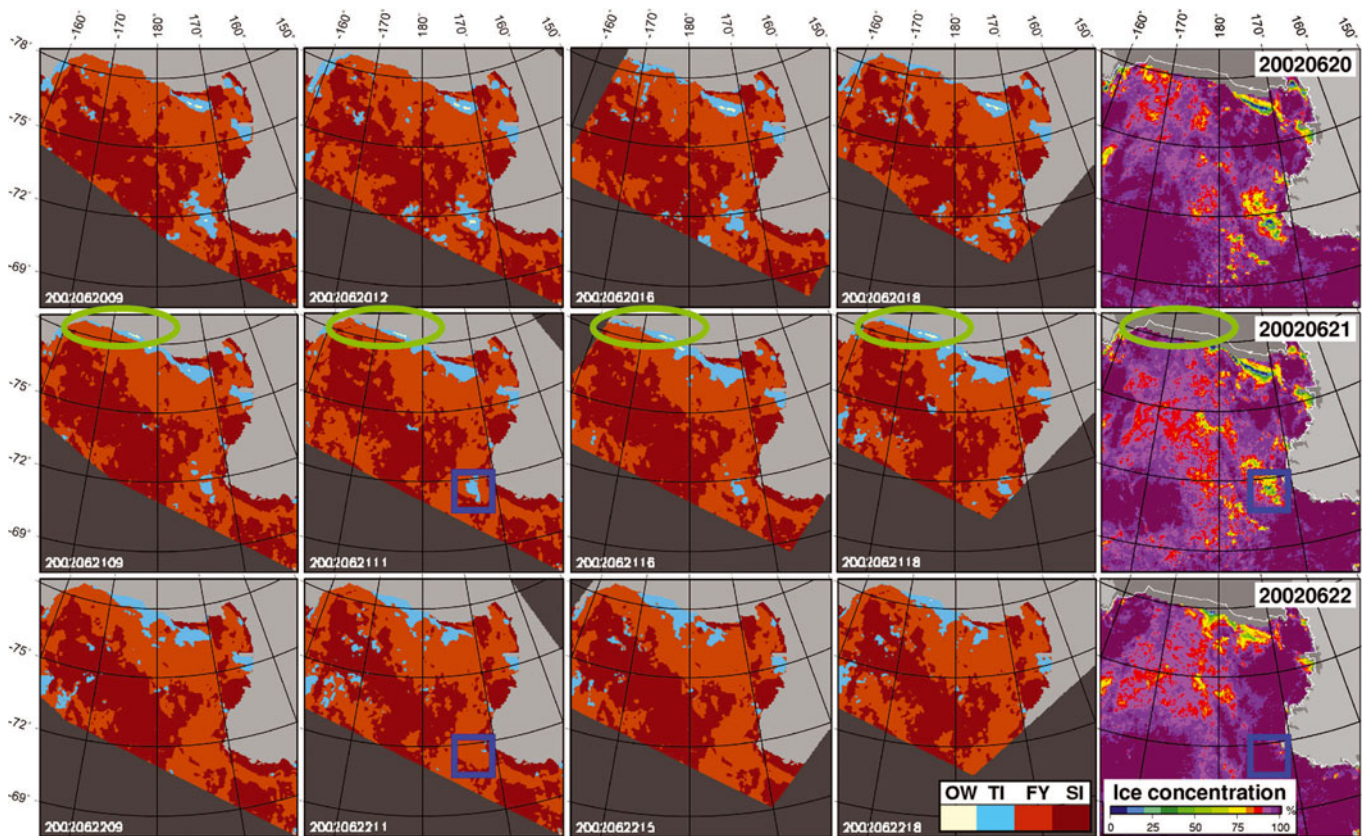


Fig. 2. Sample set of PSSM maps: open water (OW), thin ice (TI) and thick ice (FY, SI) obtained for, from top to bottom, 20, 21 and 22 June 2002, from SSM/I data of DMSP spacecraft f15 (hh: 11 or 12 and 18) and f13 (hh: 09 and 15 or 16), together with the ASI algorithm sea-ice concentration of the same day in the rightmost panel. For grey areas and date format see Figure 1; for difference between areas labelled FY and SI see Figure 6 and its discussion. Green ellipses point to discrepancies in the land–water mask and therefore polynya distribution as observed by both methods. The blue boxes highlight an example of good agreement in spatial and temporal development in a polynya as observed by both methods.

at the Mertz Glacier tongue between 145°E and 148°E dramatically decreases in size within 12 hours (Fig. 3, top row; cf. maps at 10 and 22 UTC), while a second polynya located further east (at 149°E) opens within the next

12 hours (Fig. 3, middle row, map at 09 UTC). Soon the MGP opens again along 146°E (27 June, 13 UTC), but it subsequently starts closing again and changing its orientation from zonal to meridional along 66.5°S (Fig. 3, middle

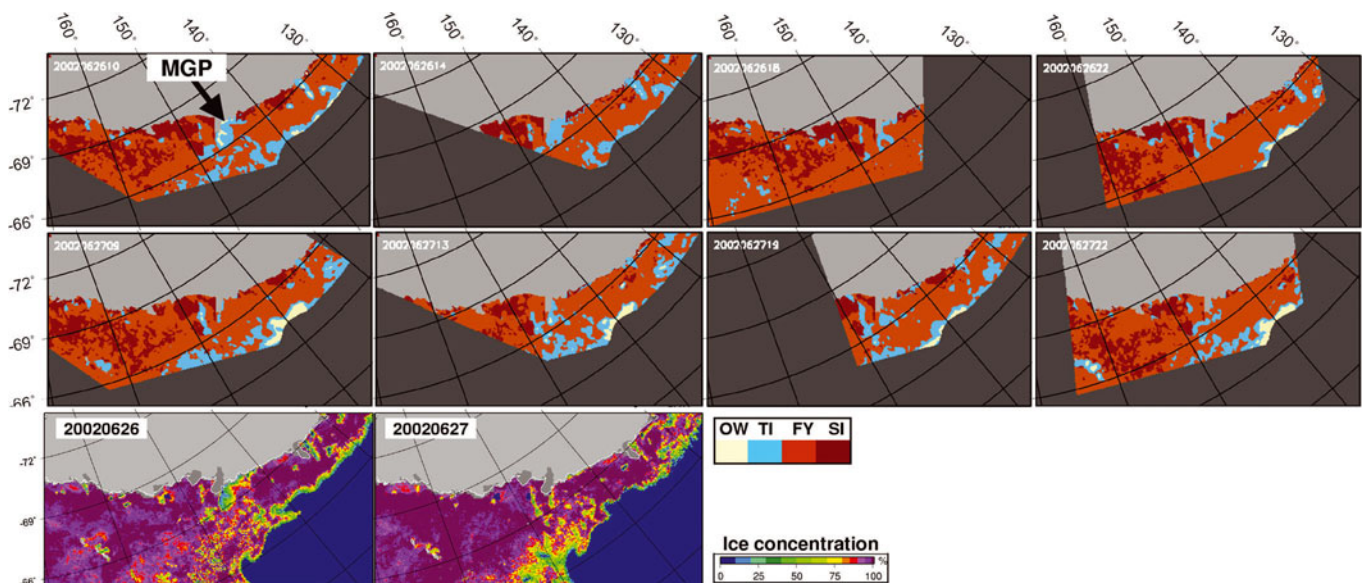


Fig. 3. Same as Figure 2, but for the MGP area (2002; top row 26 June, middle row 27 June). Size of the area: $1875\text{ km} \times 1000\text{ km}$; PSSM map (ice-concentration) grid spacing is 5 km (6.25 km).

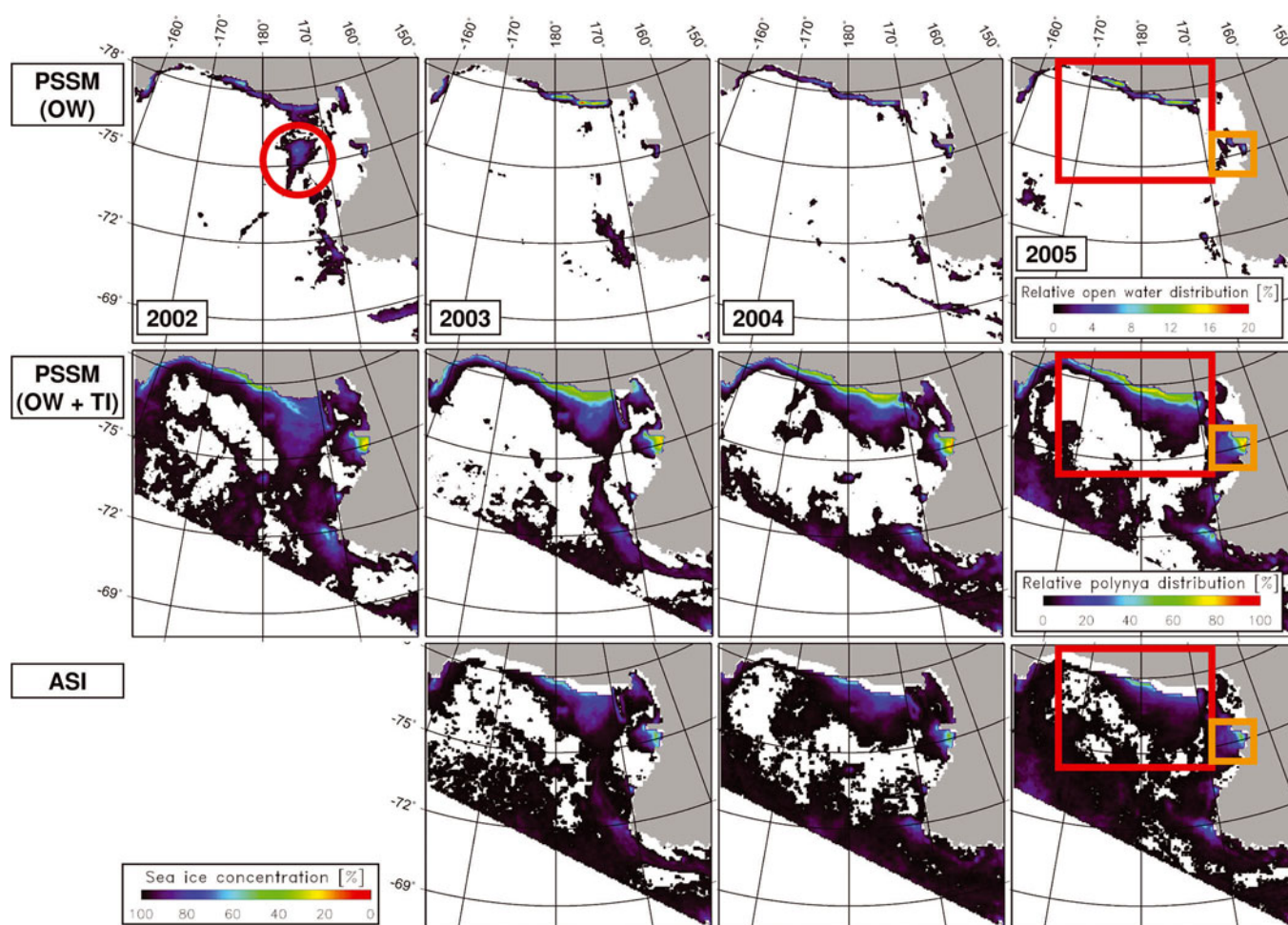


Fig. 4. Relative distribution of the open-water fraction (top) and the total polynya area (open water + thin ice) (middle) as obtained with the PSSM for winters (April–September) 2002–05 in the Ross Sea. A value of 20% in the top row means, for example, that in 20% of the selected PSSM maps (at least twice daily) open water was found. Note the different scale of two legends showing the distribution. The bottom row gives the average winter ASI algorithm sea-ice concentration calculated from all selected PSSM maps for all polynya gridcells for 2003–05. The white triangle to the bottom left in all panels denotes missing data. Areas where the relative open water or polynya distribution equals zero (top and middle row), or the sea-ice concentration equals 100% (bottom row), are also marked white. The red circle in the uppermost left panel highlights an abnormal open-water distribution. Red (orange) boxes mark the region taken for the calculation of the time series in Figure 7 for the RISP (TNBP).

row, rightmost panel, 27 June, 22 UTC). An effect by varying atmospheric water content due to a low-pressure system passing by (e.g. on 26 June) cannot be excluded totally. However, because such systems are usually associated with changes in the wind direction (easterly on 26 June, 9 UTC, becoming northerly later that day, and changing towards westerly winds on 27 June, 9 UTC) the polynya dynamics in the above example seems to be reasonable and underlines the need for sub-daily maps in regions with a very dynamic sea-ice cover (cf. Martin and others, 2004b). Oceanic tides may also play a role.

Figures 4 and 5 show the frequency distribution with which open water (top row) or a polynya in general (thin ice + open water) is observed by the SSM/I in the RISP and MGP regions for winters 2002–05, respectively. Note the remarkable change in the frequency distribution of particularly open water (red circle in uppermost left panel, Fig. 4) and the total polynya area in the RISP region between 2002 and the other three years. The reason is iceberg C19, which broke off the Ross Ice Shelf in 2002 and drifted through the western Ross Sea during 2002/03. This iceberg was oriented parallel to the ice shelf during 2002 and therefore generated

a secondary polynya on its leeward side (as can be seen in the abnormal open-water distribution in 2002). Note the high frequency of TNBP occurrence: it is observed on almost 80% of all considered days, i.e. on about 150 days in April–September. For all gridcells marked as polynya by the PSSM, the average ASI algorithm ice concentration is calculated for winters 2003–05 and is shown in comparison to the frequency distribution maps in Figures 4 and 5 at the bottom. The winter of 2002 has been omitted because of the lack of AMSR-E data for April until mid-June. All features visible in the frequency maps can be identified in the average ice concentration. Areas with a high polynya frequency show reduced ASI algorithm ice-concentration values, which tend to remain above 50% (see Table 1 and section 4 for further comments).

Figure 5 shows the open-water and total polynya area distribution for the MGP region together with the average ASI algorithm ice concentration of all polynya gridcells. The MGP turns out to be as active as the TNBP: a polynya is observed on about 80% of all considered days. However, another polynya situated further to the west at about 134° E (see black circle in uppermost left panel, Fig. 5) shows open

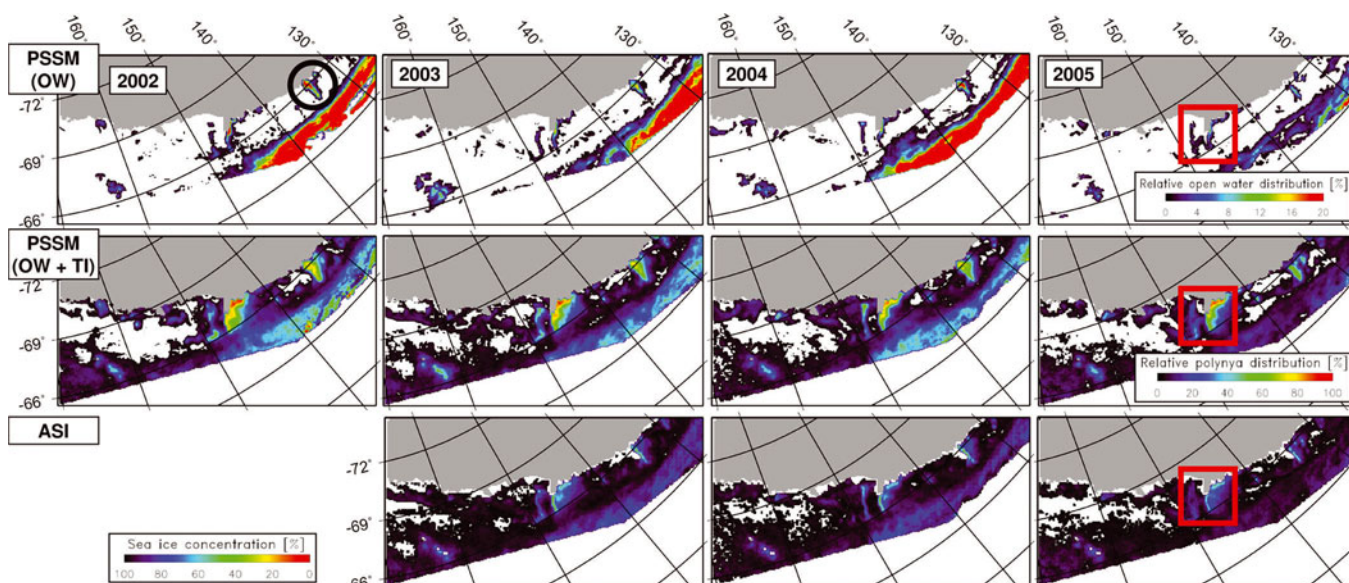


Fig. 5. Same as Figure 4, but for the MGP. The black circle highlights a second important polynya in this area.

water more frequently than the MGP. Note also that the MGP seems to be split into two parts: one directly at the glacier tongue (146° E) and the other further to the east (148° E). The high frequency of open water and polynyas towards the north (Fig. 5, top and middle rows) is an effect of the large variability of the location of the ice edge. The maps of the average ice concentration are as detailed as the polynya maps.

Motivated by question (c) in section 1, ASI algorithm ice concentrations were averaged for the three PSSM classes – open water (OW), thin ice (TI) and thick ice (FY) – for the winters of 2003–05 (e.g. for the ice concentration of the OW class, only ice-concentration values found for PSSM OW gridcells are taken). One would expect values close to 0% for OW and close to 100% for TI and FY. Table 1 reveals a different picture.

The average ice-concentration values differ considerably from expectations. Additionally there is a discrepancy between the RISP and the MGP. The average ASI algorithm ice concentration for OW (TI) is about 40–45% (78%) in the RISP and about 25% (65%) in the MGP. The corresponding values for thick ice, however, agree reasonably. The different frequencies and spatial resolutions involved in the two methods seem to be the key to explain the discrepancy between expected and observed ice-concentration values (see section 4(b)). The discrepancies between the two regions have other causes. One explanation for the higher ASI algorithm ice concentration for PSSM OW areas of the RISP compared to the MGP is the inaccurate land mask

(cf. Fig. 2, middle row). The open-water area of a coastal polynya is situated along the shore, fast-ice or shelf-ice border. An Antarctic land mask, which covers an area larger than the real land- or shelf-ice cover, potentially flags especially the open-water areas of such a polynya, and in our case of PSSM OW gridcells. The bulk of the remaining OW gridcells are probably located close to the TI area. Consequently, ASI algorithm ice concentrations can already be quite high. The polynya and therefore the OW area occupied by the inaccurate land mask is larger in the RISP compared to the MGP region, which explains the above-mentioned difference between the RISP and MGP for PSSM OW. It is unlikely that this also accounts for the difference in PSSM TI ice concentrations. Our suggestion is that this difference is caused by a difference in the prevailing ice type in the polynya (see section 4(b)).

4. ANSWERS AND DISCUSSION

This section aims at giving answers to the questions in section 1 and discusses the comparisons in section 3.

(a) Which effects must be taken into account when using the PSSM to obtain polynya area time series?

SSM/I sensors aboard different spacecraft can differ in the observed brightness temperature of the same area (e.g. Colton and Poe, 1999). In order to combine SSM/I data of DMSP-f13 and -f15 without introducing inaccuracies due to the different sensor properties, we compared DMSP-f13

Table 1. Average ASI algorithm ice concentration (in %) for PSSM open water (C(OW)), thin ice (C(TI)) and all other ice-covered gridcells (C(FY)), including class SI) for the MGP (left half) and the RISP (right half) together with one standard deviation for winters 2003–05; N is the total number of PSSM maps used. The year 2002 has been omitted because of the lack of AMSR-E data

	N , MGP	C(OW)	C(TI)	C(FY)	N , RISP	C(OW)	C(TI)	C(FY)
2003	350	29 ± 21	65 ± 12	91 ± 7	547	47 ± 26	79 ± 10	97 ± 2
2004	332	22 ± 19	63 ± 12	91 ± 5	633	39 ± 25	79 ± 9	98 ± 2
2005	328	26 ± 18	65 ± 12	92 ± 5	612	43 ± 25	76 ± 8	98 ± 2

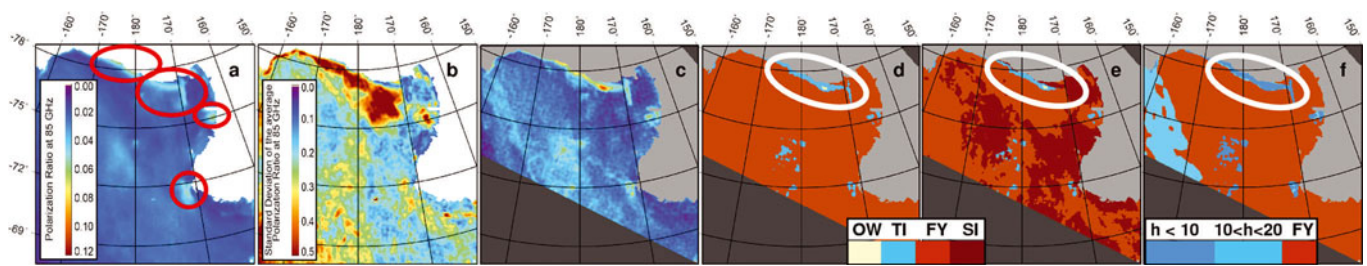


Fig. 6. (a) Average 85 GHz polarization ratio (2 weeks); (b) its variability; (c) the actual 85 GHz polarization ratio (7 June 2002, 12 UTC); (d) the resulting PSSM map; (e) the same, but after applying the mentioned mask (see text); and (f) polynya distribution after the method of Ohshima and others (2005), with h the ice thickness in centimetres. Note that the polynyas and tabular icebergs (cf. Fig. 1) encircled red in (a) exhibit similar elevated values of the 85 GHz polarization ratio for icebergs and polynyas. White ellipses in (d–f) mark the region where application of the SI mask mitigates misclassifications of icebergs and fast ice as thin ice by the PSSM, while these are classified as ice <10 cm thickness in the map of Ohshima.

and -f15 SSM/I 37 GHz and 85 GHz brightness temperatures of three different regions (each 90 000 km²) of the inner Antarctic during winter (June–July). A linear regression is carried out (correlation coefficient 0.978, rms error 1.2 K), which is subsequently used to transform DMSP-f13 SSM/I data onto the level of DMSP-f15. The magnitude of this transformation is equivalent to a difference in the polarization ratio of 0.003, which amounts to 10% of a typical value for first-year ice: 0.03. A close inspection of the effect upon the PSSM maps derived using DMSP-f13 and -f15 SSM/I data revealed negligible differences.

Fast ice and tabular icebergs may be misinterpreted as thin ice. This is caused by an on average higher polarization ratio compared to first-year ice. This is particularly important because polynyas form quite often along the fast-ice border or in the lee of a tabular iceberg (see Fig. 1). Therefore a reliable discrimination between fast ice/tabular icebergs and thin ice/open water is required. This is realized by applying a mask, called a stable ice mask henceforth, which excludes all areas from the PSSM map that have high (compared to first-year ice) and temporally stable values of the polarization ratio at 85 GHz. For this mask, the 85 GHz polarization ratio is temporally averaged over 2 weeks ending at the day of interest for each gridcell (Fig. 6a). A threshold is applied to the resulting map, which selects areas with an average 85 GHz polarization ratio that is higher than that of first-year ice; the threshold is selected such that the selected area contains fast ice, shelf ice, icebergs and thin ice/open water (i.e. polynya area). In order to separate the polynya area from the other types mentioned, this map is combined with the map of the temporal variability over the same period (Fig. 6b). By assuming that on a scale of 2 weeks the 85 GHz polarization ratio has a larger temporal variability over a polynya compared to fast ice/shelf ice/icebergs, the latter three types can be separated and put into the stable ice (SI) mask. This mask is subsequently applied to the PSSM maps. Figure 6d and e show how this mask (Fig. 6e, class SI) successfully masks the two tabular icebergs (B15 and C19; cf. Fig. 1) in the RISP area, which can be identified in Figure 6c by an 85 GHz polarization ratio of around 0.045, and which therefore are classified as thin ice (Fig. 6d). The method of Ohshima and others (Fig. 6f) misclassifies the icebergs as thin ice of <10 cm thickness. The SI mask also flags areas with a temporally stable ‘normal’ sea-ice cover.

Finally, when studying coastal polynyas it is essential to use a land mask, which is as accurate and actual as possible, because of the often quite small across-polynya extent. This

is particularly difficult for the Antarctic because of the variable shelf-ice borders. Therefore, we updated the land mask, which is provided by the NSIDC (1996) and which contains land and shelf ice, by overlying clear-sky AVHRR visible and IR temperature images, interpolated on the same fine-meshed version of the NSIDC grid (5 km by 5 km gridcell size) as the 85 GHz SSM/I data used in the PSSM, onto the old land mask, and correcting the latter manually for the discrepancy in the coastline and shelf-ice borders (not shown).

(b) At what ice thickness do the PSSM thin-ice areas terminate?

To answer this question, we first have to discuss the discrepancies between the PSSM and the ASI algorithm given in Table 1. The classification used in the PSSM is carried out using typical values for the average polarization ratio of thin ice, open water and first-year ice. While the latter is calculated every day from areas with >90% sea-ice concentration, the other two are selected from a set of typical values after comparison of the obtained PSSM maps with independent data (e.g. AVHRR data) and remain fixed at 0.085 and 0.18 for thin ice and open water, respectively. Such a fixed value, particularly for thin ice, however, is also valid for an open-water/(thick-)ice mixture. Therefore, thin-ice areas detected by the PSSM are ambiguous in that they can resemble 100% thin ice or such a mixture (e.g. pancake ice bands). The latter are typical for the ice edge (e.g. Doble and others, 2003), but are also found quite regularly in coastal polynyas. First, typically frazil and grease ice forms, which is advected by the surface wind to the leeward side of the opening. Depending on wind speed and fetch and air temperature, this ice either accumulates to form thin level ice or it organizes itself into rows of densely packed pancakes. While these rows can be discriminated in a synthetic aperture radar (SAR) or IR temperature image (e.g. Drucker and others, 2003), it is not possible to resolve them using SSM/I data. However, the finer spatial resolution achieved with the AMSR-E (e.g. using the ASI algorithm) could enable discrimination between such open-water/pancake-ice areas. Therefore, thin-level-ice and pancake-ice bands with intermitted open water result in the same PSSM pattern but could cause different ice concentrations using AMSR-E 89 GHz data and the ASI algorithm: for example, 100% for thin level ice and around 60–80% (or even less) when pancake-ice bands dominate. We suggest that this capability of the ASI algorithm when applied to

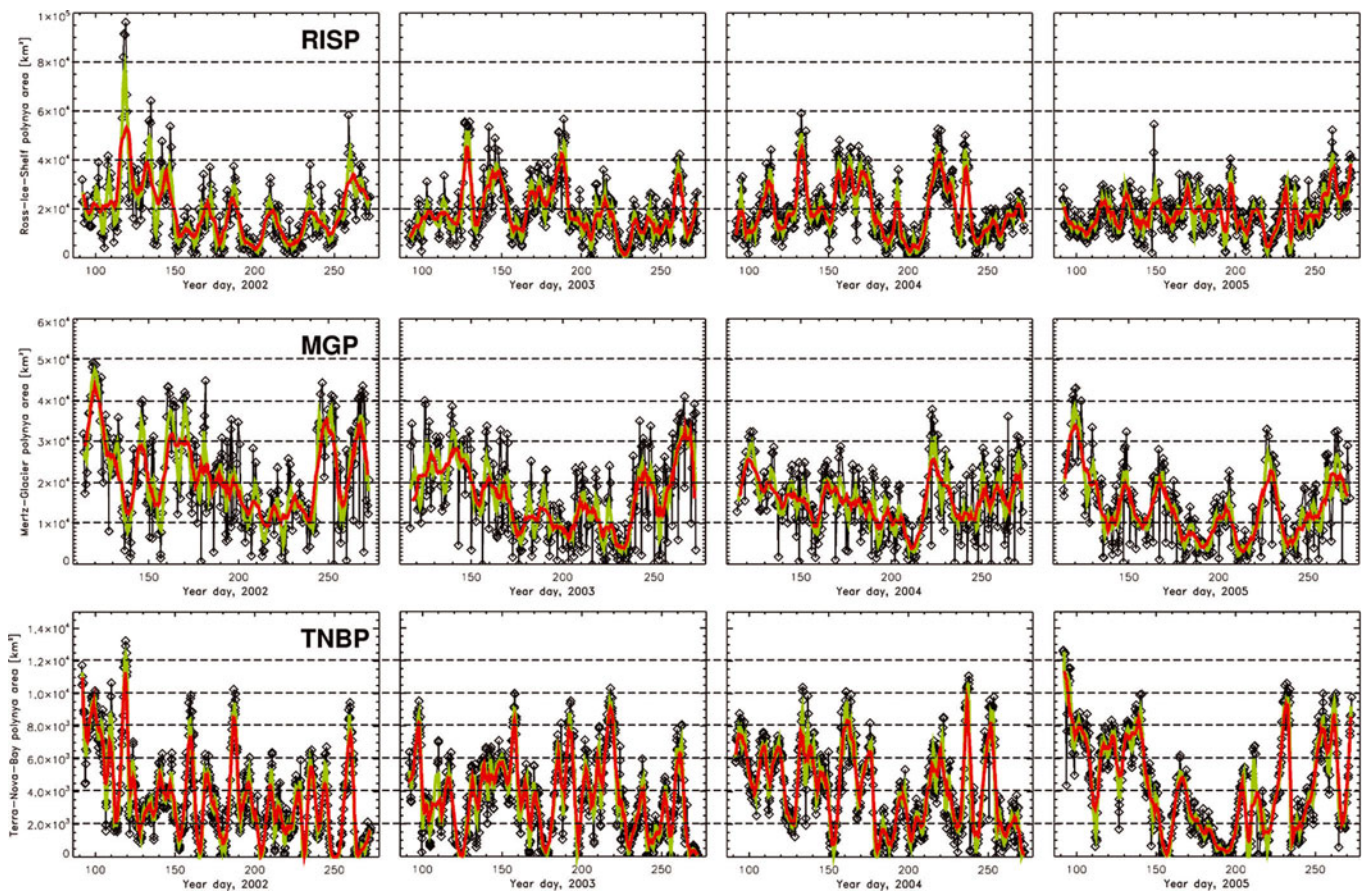


Fig. 7. Time series of the total polynya area for 2002–05 for the RISP (top), MGP (middle) and TNBP (bottom). Black symbols connected by lines are the single (at least twice-daily) observation of the polynya area. Green and red lines mark the running mean of the observed polynya area over 3 and 7 days, respectively. Note the different time axis used for the MGP and the RISP/TNBP. Note the different scaling of the y axis.

AMSR-E 89 GHz is the key to explain the unexpectedly low ASI algorithm ice-concentration values for the PSSM TI areas (Table 1). Further, thin level ice becomes optically thick at a smaller thickness at 89 GHz (5 mm) compared to 37 GHz (20 mm). These values increase for grease ice and first forms of pancake ice due to the less defined vertical salinity profile. It is therefore likely that the PSSM OW area contains a considerable amount of frazil/grease ice, which is difficult to quantify. We suggest that this uncertainty in the PSSM maps is the key to explain the unexpectedly high ASI algorithm ice-concentration values for the PSSM OW areas (Table 1).

Because the PSSM seems to be independent of (thin-)ice type it is difficult to assign a typical maximum ice-thickness value to PSSM TI areas. However, according to our thermal ice-thickness calculations (see Fig. 1) and the results of Martin and others (2004a), we also suggest a value of 20–25 cm. This has to be regarded as an area average thickness. Following the above considerations about the typical ice thickness at which level or grease ice becomes optically thick at 37 GHz, it makes sense to suggest a value of 5 cm as a lower (upper) thickness limit for the PSSM TI (OW) class.

(c) What additional information can we obtain from high-resolution AMSR-E 89 GHz ice-concentration estimates?

Most of this question is answered in section 4(b). AMSR-E 89 GHz data allow a finer spatial resolution and a more

reliable detection of open water due to an increased sensitivity to thin ice, as is possible using SSM/I 37 GHz data (even at a finer grid spacing). Therefore, the ASI algorithm could be used to identify open water more reliably within the PSSM polynya area. Further, it could be used to obtain information about the ice type within the PSSM TI area: ASI algorithm ice concentrations close to 100% indicate thin level ice; values considerably below 100% indicate pancake ice. This might be a topic of future studies.

5. POLYNYA VARIABILITY

Figure 7 shows time series of the total polynya area derived from the PSSM maps for the subregions shown by the red (and orange) boxes in Figures 4 and 5: the RISP, MGP and TNBP. Each time series consists on average of twice-daily observations of DMSF-f15 SSM/I. The total area of the RISP varies typically between zero and 40 000–60 000 km²; no notable difference can be identified between the years shown. The wintertime mean of the open-water area and total polynya area takes values between about 450 km² (2004) and 800 km² (2002), and between 18 300 km² (2005) and 19 400 km² (2004), respectively. The total area of the TNBP varies between zero and about 10 000 km². The mean winter open-water area and total polynya area varies between 40 km² (2003) and 110 km² (2004), and between 3600 km² (2002) and 4400 km² (2005), respectively. The RISP and TNBP total polynya areas together amount to about

22 000 km². This is slightly more than the area, 20 000 km², observed by Arrigo and Van Dijken (2003) during winter for the entire Ross Sea, i.e. including the polynyas outside the red and orange boxes in Figure 4. Why is our area larger, although it has been obtained from a smaller region? Arrigo and Van Dijken (2003) used a different technique to estimate the polynya area, which yields a smaller total polynya area than the PSSM. Parmiggiani (2006) defined the area of the TNBP using a concentration threshold of 70% applied to AMSR-E ice-concentration maps. He obtained values of the daily average total polynya area for 13, 17, 20 and 25 September 2003, of 200, 5600, 6300 and 200 km², which agree reasonably with our estimates of 100, 7000, 7200 and 150 km², taking into account the different techniques used.

The total area of the MGP varies typically between zero and 25 000–45 000 km². The mean winter open-water area and total polynya area takes values between 350 km² (2002, 2004) and 950 km² (2003), and between 13 600 km² (2005) and 22 000 km² (2002), respectively. The total MGP area agrees within one standard deviation with earlier findings (Massom and others, 1998). There seems to be a downward trend in MGP area during the first half/two-thirds of winter, with a minimum polynya area in August. This is similar to the results of Arrigo and Van Dijken (2003) and could be explained by the increasing amount of ice downwind of the polynya and thus the larger force required to push the ice away from the coast. The mean change in the polynya area between successive (i.e. on a sub-daily timescale) DMSP-SSM/I overpasses, which completely cover the boxes denoting the subregions (see Figs 4 and 5) (at least one ascending and one descending overpass), amounts to 5800 km² (MGP) and 4500 km² (RISP), but only to 800 km² in the TNBP; it may amount to 20 000 km² in the MGP and the RISP but is only 2000 km² in the TNBP. Extreme area changes occur more often in the MGP than in the RISP and TNBP, which could be an effect of a stronger influence of weather systems for the MGP compared to the RISP and TNBP. The TNBP area appears to be much more stable on this sub-daily timescale. This is confirmed by Figure 4, where the relative polynya distribution exceeds 80% in the TNBP in each of the years 2002–05. Like the MGP, the TNBP is forced by katabatic winds (Bromwich and Kurtz, 1984), which, however, could be expected to be much more persistent in the TNBP than in the MGP due to the more sheltered location of the TNBP.

The running-mean total polynya area calculated for periods of 3 and 7 days (Fig. 7, green and red lines) reveals that major MGP area changes tend to occur at shorter time intervals (at least in 2002–04) than major RISP and TNBP area changes. However, changes at short (3 day) as well as long (20 day) intervals occur in both regions; compare the RISP in 2002 and 2005 and the MGP for the same years. Therefore, although the RISP is sheltered in the Ross Sea, and the MGP is frequently influenced by cyclones, the polynya area time series shown do not allow a definite conclusion about different typical timescales of the polynya dynamics on a daily to weekly scale. Major changes in the TNBP seem to occur on a scale of 7–10 days, at least during 2002–04.

6. CONCLUSIONS

By applying the PSSM to DMSP-f13 and -f15 SSM/I data of the winters (April–September) of 2002–05, an analysis was made of the polynyas in the Ross Sea and off the Adélie

Coast. The most prominent polynyas, the RISP, the TNBP and the MGP, were investigated. A new land mask resulting from manual AVHRR imagery analysis was used. Maps of the mean frequency distribution for the occurrence of open water and the entire polynya area were obtained for the Ross Sea and the region off the Adélie Coast. These reveal that the break-up and drift of the tabular iceberg C19 from the Ross Ice Shelf has caused a different polynya distribution in the RISP region in 2002 as compared to the other three winters, by the generation of a secondary polynya in its lee. Mean winter areas of these polynyas range from 18 300 to 19 400 km² (RISP), 3600 to 4400 km² (TNBP) and 13 600 to 22 000 km² (MGP), while extreme areas reach 96 000 km² (RISP), 10 100 km² (TNBP) and 49 500 km² (MGP). The RISP and TNBP differ from the MGP in the amount of day-to-day changes: about 4500 km² (RISP), 800 km² (TNBP) and about 5800 km² (MGP). This underlines the persistence of the katabatic winds forcing the TNBP, while those forcing the MGP are less persistent due to the frequent influence of weather systems. No definitive timescale for major changes in the total polynya area was found; typical time intervals range from 3 to 20 days in all polynyas. An examination of these time series together with a time series of the surface wind vector would be required for further conclusions, ideally also for a longer time period. Because of a similar microwave radiometric signature of fast ice/icebergs/ice shelves compared to thin ice, a new mask was developed, which utilizes the temporal evolution of this signature over the past 2 weeks. It was shown that this mask allows 85% of false TI areas to be discarded from the PSSM analysis. It may be necessary to carry out an inter-spacecraft (e.g. DMSP-f13 to -f15) sensor correction when the goal is to combine SSM/I data of both spacecraft. This would be important for studies of the sub-daily polynya dynamics as well as of the long-term polynya area development.

AMSR-E ASI algorithm ice-concentration maps are currently the concentration product with the finest spatial resolution. Since this resolution is comparable to the gridcell size of the PSSM maps, a combination of the two methods would certainly be of use for future applications. It was shown that, on average, the polynya distribution as given by the average ASI-algorithm ice concentration of all polynya area gridcells is similar to that given by the PSSM. Average ice concentrations calculated separately for the PSSM OW and TI classes take values of around 25% (45%) and 65% (78%) for the MGP (RISP) regions, respectively. The reasons for the discrepancy between expected (0% and 100% for OW and TI) and observed ASI algorithm ice concentration are discussed. The PSSM OW area likely contains a considerable amount of frazil/grease ice, which causes non-zero ice concentrations when using the ASI algorithm because of the higher sensitivity to thin ice at the higher frequency used. The PSSM classifies 100% thin-level-ice and pancake-ice bands with intermitted open water similarly to thin ice, while the ASI algorithm seems to be capable of distinguishing between the two ice types. A combination of PSSM and ASI algorithm could be used to more reliably identify open water and differentiate between level and pancake ice in a polynya, but this requires further investigation.

We included thermal ice thickness derived using AVHRR IR temperature observations and ERA-40 atmospheric data in our analysis. The good agreement between the ice-thickness distribution and PSSM maps for quite a number of

cases suggests using this distribution to obtain an upper thickness limit for the PSSM TI area: 20–25 cm. However, in the light of the numerous possible error sources, we restricted the ice-thickness analysis to 2002 and intend to take these estimates as the starting point for an analysis of the RISP and MGP regions similar to the work of Martin and others (2004a).

ACKNOWLEDGEMENTS

This work was supported by the German Science Foundation (DFG): Me 487/40-1 and 40-2. The helpful comments of two anonymous reviewers are gratefully acknowledged.

REFERENCES

- Arrigo, K.R. and G.L. Van Dijken. 2003. Phytoplankton dynamics within 37 Antarctic coastal polynya systems. *J. Geophys. Res.*, **108**(C8), 3271. (10.1029/2002JC001739.)
- Bromwich, D.H. and D.D. Kurtz. 1984. Katabatic wind forcing of the Terra Nova Bay polynya. *J. Geophys. Res.*, **89**(C3), 3561–3572.
- Cavaliere, D.J. 1994. A microwave technique for mapping thin sea ice. *J. Geophys. Res.*, **99**(C6), 12,561–12,572.
- Colton, M.C. and G.A. Poe. 1999. Intersensor calibration of DMSP SSM/I's: F-8 to F-14, 1987–1997. *IEEE Trans. Geosci. Remote Sens.*, **37**(1), 418–439.
- Doble, M.J., M.D. Coon and P. Wadhams. 2003. Pancake ice formation in the Weddell Sea. *J. Geophys. Res.*, **108**(C7), 3029–3030.
- Drucker, R., S. Martin and R. Moritz. 2003. Observations of ice thickness and frazil ice in the St. Lawrence Island polynya from satellite imagery, upward looking sonar, and salinity/temperature moorings. *J. Geophys. Res.*, **108**(C5), 3149. (10.1029/2001JC001213.)
- Gordon, A.L. and J.C. Comiso. 1988. Polynyas in the Southern Ocean. *Sci. Am.*, **258**(6), 70–77.
- Hunewinkel, T., T. Markus and G.C. Heygster. 1998. Improved determination of the sea ice edge with SSM/I data for small-scale analyses. *IEEE Trans. Geosci. Remote Sens.*, **36**(5), 1795–1808.
- Kaleschke, L. and 6 others. 2001. SSM/I sea ice remote sensing for mesoscale ocean–atmosphere interaction analysis. *Can. J. Remote Sens.*, **27**(5), 526–537.
- Källberg, P.W., A.J. Simmons, S. Uppala and M. Fuentes. 2004. *The ERA-40 archive*. Reading, European Centre for Medium-Range Weather Forecasts. (ERA-40 Project Report Series, 17.)
- Kern, S., I.H. Harms, S.A. Bakan and Y. Chen. 2005. A comprehensive view of Kara Sea polynya dynamics, sea-ice compactness and export from model and remote sensing data. *Geophys. Res. Lett.*, **32**(15), L15501. (10.1029/2005GL023532.)
- Key, J. 2002. *The Cloud and Surface Parameter Retrieval (CASPR) system for polar AVHRR. User's guide, version 4.0*. Madison, WI, University of Wisconsin. Cooperative Institute for Meteorological Satellite Studies.
- Key, J.R., J.B. Collins, C. Fowler and R.S. Stone. 1997. High-latitude surface temperature estimates from thermal satellite data. *Remote Sens. Environ.*, **61**(2), 302–309.
- Lemke, P. 2001. Open windows on the polar oceans. *Science*, **292**(5522), 1670–1671.
- Markus, T. and B.A. Burns. 1995. A method to estimate sub-pixel-scale coastal polynyas with satellite passive microwave data. *J. Geophys. Res.*, **100**(C3), 4473–4487.
- Markus, T., C. Kottmeier and E. Fahrbach. 1998. Ice formation in coastal polynyas in the Weddell Sea and their impact on oceanic salinity. In Jeffries, M.O., ed. *Antarctic sea ice: physical processes, interactions and variability*. Washington, DC, American Geophysical Union, 273–292. (Antarctic Research Series 74.)
- Marsland, S.J., N.L. Bindoff, G.D. Williams and W.F. Budd. 2004. Modeling water mass formation in the Mertz Glacier Polynya and Adélie Depression, East Antarctica. *J. Geophys. Res.*, **109**(C11), C11003. (10.1029/2004JC002441.)
- Martin, S., R. Drucker, R. Kwok and B. Holt. 2004a. Estimation of the thin ice thickness and heat flux for the Chukchi Sea Alaskan coast polynya from Special Sensor Microwave/Imager data. *J. Geophys. Res.*, **109**(C10), C10012. (10.1029/2004JC002428.)
- Martin, S., I. Polyakov, T. Markus and R. Drucker. 2004b. Okhotsk Sea Kashevarov Bank polynya: its dependence on diurnal and fortnightly tides and its initial formation. *J. Geophys. Res.*, **109**(C9), C09S04. (10.1029/2003JC002215.)
- Massom, R.A., P.T. Harris, K.J. Michael and M.J. Potter. 1998. The distribution and formative processes of latent-heat polynyas in East Antarctica. *Ann. Glaciol.*, **27**, 420–426.
- National Snow and Ice Data Center (NSIDC). 1996. *DMSP SSM/I brightness temperatures and sea ice concentration grids for polar regions: user's guide – revised edition*. Boulder, CO, University of Colorado. Cooperative Institute for Research in Environmental Sciences. National Snow and Ice Data Center.
- Ohshima, K.I., S. Nishihashi and T. Tamura. 2005. Detection of coastal polynyas and ice production in the Antarctic and Okhotsk Seas from SSM/I. In *IGARSS '05. 25th International Geoscience and Remote Sensing Symposium, 25–29 July 2005, Seoul, Korea. Proceedings, Vol. 4*. Piscataway, NJ, Institute of Electrical and Electronics Engineers, 2652–2655.
- Parmiggiani, F. 2006. Fluctuations of Terra Nova Bay polynya as observed by active (ASAR) and passive (AMSR-E) microwave radiometers. *Int. J. Remote Sensing*, **27**(12), 2459–2467.
- Spreen, G., L. Kaleschke and G. Heygster. In press. Sea ice remote sensing using AMSR-E 89 GHz channels. *J. Geophys. Res.*
- Stössel, A. and T. Markus. 2004. Using satellite-derived ice concentration to represent Antarctic coastal polynyas in ocean climate models. *J. Geophys. Res.*, **109**(C2), C02014. (10.1029/2003JC001779.)
- Svendsen, E., C. Mätzler and T.C. Grenfell. 1987. A model for retrieving total sea ice concentration from a spaceborne dual-polarized passive microwave instrument operating near 90 GHz. *Int. J. Remote Sensing*, **8**(10), 1479–1487.
- Van Woert, M.L. 1999. Wintertime dynamics of the Terra Nova Bay polynya. *J. Geophys. Res.*, **104**(C4), 7753–7769.
- Yu, Y. and D.W. Lindsay. 2003. Comparison of thin-ice distributions derived from RADARSAT Geophysical Processor System and advanced very high resolution radiometer data sets. *J. Geophys. Res.*, **108**(C12), 3387–3388.